Int. J. Electrochem. Sci., 11 **(2016)** 4743 – 4754, doi: 10.20964/2016.06.22

International Journal of
ELECTROCHEMICAL
SCIENCE
www.electrochemsci.org

Nitrogen-doped Porous Carbon Derived from Rapeseed residues for High-performance Supercapacitors

Kanjun Sun[1,*], *Dongyang Guo*[2], *Xiaoping Zheng*[1], *Yanrong Zhu*[1], *Yanping Zheng*[1], *Mingguang Ma*[1], *Guohu Zhao*[1], *Guofu Ma*[2,*]

[1] College of Chemistry and Environmental Science, Lanzhou City University, Lanzhou 730070, China.
[2] Key Laboratory of Eco-Environment-Related Polymer Materials of Ministry of Education, Key Laboratory of Polymer Materials of Gansu Province, College of Chemistry and Chemical Engineering, Northwest Normal University, Lanzhou 730070, China.
[*]E-mail: sunkj@lzcu.edu.cn; magf@nwnu.edu.cn

Received: 4 December 2015 / *Accepted:* 30 March 2016 / *Published:* 4 May 2016

In this paper, nitrogen-doped activated carbons obtained from rapeseed residues (N-RCs) as supercapacitor electrodes are successfully synthesized by a simple chemical activation method. The field emission scanning microscope, transmission electron microscopy, and N_2 adsorption-desorption tests demonstrate that N-RCs treated with $ZnCl_2$ can produce a large number of mesopores. Additionally, the N-RCs have certain amount of nitrogen (nitrogen content in N-RC2 is 6.55% by element content analysis). As the electrode material, N-RC2 exhibits ideal capacitive behavior in 6 mol L^{-1} KOH aqueous electrolyte in a three-electrode system tests, and the maximum specific capacitance reaches 250 F g^{-1} at a current density of 0.5 A g^{-1}. Furthermore, in 0.5 mol L^{-1} Na_2SO_4 aqueous electrolyte, the as-assembled N-RC2//N-RC2 symmetric cell exhibits high energy density of 13.55 Wh kg^{-1} at a power density of 399.80 W kg^{-1} operated at the voltage range of 0 to 1.8 V and an excellent cycleability retaining about 92.8% initial capacitance after 5000 cycles.

Keywords: Rapeseed residues, Activated carbon, Nitrogen-doped, Supercapacitor

1. INTRODUCTION

As a new class of efficient energy storage device, supercapacitors with high power density, excellent cycling stability, wide operation temperature range, and high safety are now attracting extensive attention for many portable systems and hybrid electric vehicles [1-5]. Supercapacitors are categorized into electric double-layer capacitors (EDLCs) that store electric energy by the physical adsorption of electrolyte ions onto a charged electrode via electrostatic attraction, such as carbon

materials, and pseudocapacitors that mainly derive their energy storage capacity from reversible faradaic reactions at the surface of active material, such as metal oxides and conductive polymers [6-8]. However, low electrical conductivity, poor cycle stability and high price have limited the practical application of those pseudocapacitive materials [9-11]. Carbon materials, especially the activated carbons, remaining the most common and important electrode candidates for supercapacitors due to their outstanding cycleability, porous structure with a large surface area, high conductivity, low-cost, and availability [12-14]. Nitrogen-doped porous carbon materials, from the viewpoint of practical application, have been found to cause an increase in electric conductivity, and concurrently ameliorate surface wettability as well as adsorption properties that facilitate an electrochemical reaction on the carbon surface, thus improving the electrochemical performance of electrode materials, and have been proved to be intriguing electrode materials for supercapacitors [15-18]. Nitrogen-doped carbons are prepared by two primary pathways, utilizing nitrogen-containing precursors or post-treatment of carbons. The first method is by in situ doping precursors with abundant nitrogen, which can facilitate the uniform incorporation of nitrogen into the carbon materials with controlled chemistry. Up to now, various nitrogen-containing precursors have been investigated to prepare nitrogen-doped carbons [19-21]. In contrast, for the latter, the carbon materials are treated with chemical agents, including ammonia [22] or urea [23]. Through this method, the nitrogen-containing functional groups are located on the surface and do not change the properties of the raw materials. However, many severe drawbacks, such as the complex process, low yield and high cost in the preparation still prevent widespread and practical use of nitrogen-doped carbon materials in commercial supercapacitors. Therefore, it is significant to find an easy method and a new precursor that is environmental friendly, cheap and high nitrogen content to make nitrogen-doped carbon materials.

Recycling of waste products for synthesis of activated carbon-based supercapacitor electrodes has attracted increasing attention recently [24, 25]. Actually many waste products such as newspaper, wood, tire, and banana peel are potential sources of activated carbons. For example, Lee et al. have reported that using recycled waste paper as a new source of raw material for electric double-layer capacitors achieving a maximum specific capacitance of 180 F g^{-1} at a 2 mV s^{-1} scan rate [26]. Rufford et al. synthesized activated carbon of excellent performance derived from waste coffee grounds in an aqueous EDLC operating up to 1.2 V, and an energy density of 34 Wh kg^{-1} at low current loads could be gained [27]. Ming et al. presented an effective synthetic method that utilized waste tires as the precursor to prepare the activated carbon electrodes by the pyrolysis and chemical activation processes [28]. Rapeseed residues, which are the solid residue remaining after extraction of the oil from the rapeseed, are the most commonly preferred in animal feed because they contain 16-24% protein. Therefore, it is significant to generate nitrogen-doped activated carbons that have a wide range of use and high additional value from rapeseed residues. In this paper, we present an effective synthetic route to prepare activated carbons from the recycled rapeseed residues through a simple chemical activation method, and the nitrogen-doped rapeseed residues activated carbons (N-RCs) were activated by $ZnCl_2$ to improve their surface performances and pore structures. The influence of chemical activation on the surface characteristics and capacitances of activated carbon samples were observed, as well as the three-electrode and two-electrode cells were fabricated to assess the electrochemical performance of N-RCs electrodes.

2. EXPERIMENTAL

2.1. Materials

Rapeseed residues were collected from the local oil mill, zinc chloride ($ZnCl_2$, Aladdin Ltd., Shanghai, China). All chemical reagents were in analytical grade.

2.2. Synthesis of nitrogen-doped rapeseed residues activated carbons (N-RCs)

In a typical synthesis, the mixtures of rapeseed residues and $ZnCl_2$ in different ratios (Rapeseed residues/$ZnCl_2$ mass proportion is 1:0, 1:0.5, 1:1, 1:1.5, respectively) were placed in a porcelain boat and loaded into a quartz tube furnace, heated up to the ultimate temperature of 700 °C under a high pure N_2 atmosphere with a heating rate of 5 °C min^{-1}, allowed to dwell in that temperature for 2 h, and then followed by cooling down to room temperature. After then, the resulting samples were washed with 2 mol L^{-1} HCl, and then washed with distilled water for several times until neutral pH, and finally dried in vacuum at 60 °C for 24 h. The samples of different activation proportions with $ZnCl_2$ were denoted as N-RC0, N-RC1, N-RC2 and N-RC3, respectively.

2.3. Three-Electrode Cell Fabrication

For a three-electrode system, the working electrode was fabricated with a 5 mm diameter glassy carbon electrode, the method was similarly to our previous reported literature [29]. Typically, 4.0 mg of N-RCs was ultrasonically dispersed in 0.4 mL of 0.25 wt% Nafion (DuPont, Wilimington, DE, U.S.A.) ethanol solution. The uniform suspension of 8 μL was dropped onto the surface of a glassy carbon electrode using a pipet gun and dried at room temperature naturally. The three-electrode system was tested in 6 mol L^{-1} KOH aqueous electrolyte, carbon rod electrode serves as the counter electrode and Hg/HgO as the reference electrode, respectively.

2.4. Two-Electrode Cell Fabrication

For a typical two-electrode system, the working electrode was prepared by mixing the N-RC2 with commercial carbon black and polymer binder (polyvinylidene fluoride) (8:1:1) and homogenizing slurry in N-methyl-2-pyrrolidone solution. Then, the slurry was coated on nickel foam with a working area of 1.0 cm^2 and the electrodes were dried at 60 °C for 24 h, weighted and pressed into sheets under 15 MPa. The total mass of each electrode was between 3.0 and 5.0 mg and we chose the two electrodes with identical or very close weight for the measurements [30]. The N-RC2 electrode fitted with the separator (thin polypropylene film) and electrolyte solution were symmetrically assembled into electrode/separator/electrode construction (sandwich-type cells). Before being assembled into the supercapacitor configuration, the N-RC2 electrodes and separator were immersed in 0.5 mol L^{-1} Na_2SO_4 electrolytes for 12 h to make aqueous electrolyte solutions homogeneously diffuse into the N-RC2 electrodes.

2.5. Characterization and electrochemical measurement

The morphologies and structures of the carbon samples were examined by a field emission scanning microscope (FE-SEM, Ultra Plus, Carl Zeiss, Germany) and transmission electron microscopy (TEM, JEM-1200EX, 200 kV). X-ray diffraction (XRD) of samples was performed by a diffractometer (D/Max-2400, Rigaku). Raman spectra were recorded with an in Via Raman spectrometer (Renishaw) with an argon ion laser (λ = 514 nm). The Brunauer-Emmett-Teller (BET) surface area (SBET) of the samples was analyzed by nitrogen adsorption in a Micromeritics ASAP 2020 nitrogen adsorption apparatus (U.S.A.). The elemental microanalysis (C, H and N) was carried out using the Elemental Analyzer Vario EL.

The electrochemical properties of the electrodes were investigated by cyclic voltammetry (CV), galvanostatic charge/discharge and electrochemical impedance spectroscopy (EIS) measurements in three-electrode cell using a CHI 660D electrochemical workstation. The cycle-life stability was performed using computer controlled cycling equipment (LAND CT2001A, Wuhan China).

3. RESULTS AND DISCUSSION

3.1. The morphologies and structures of N-RCs samples

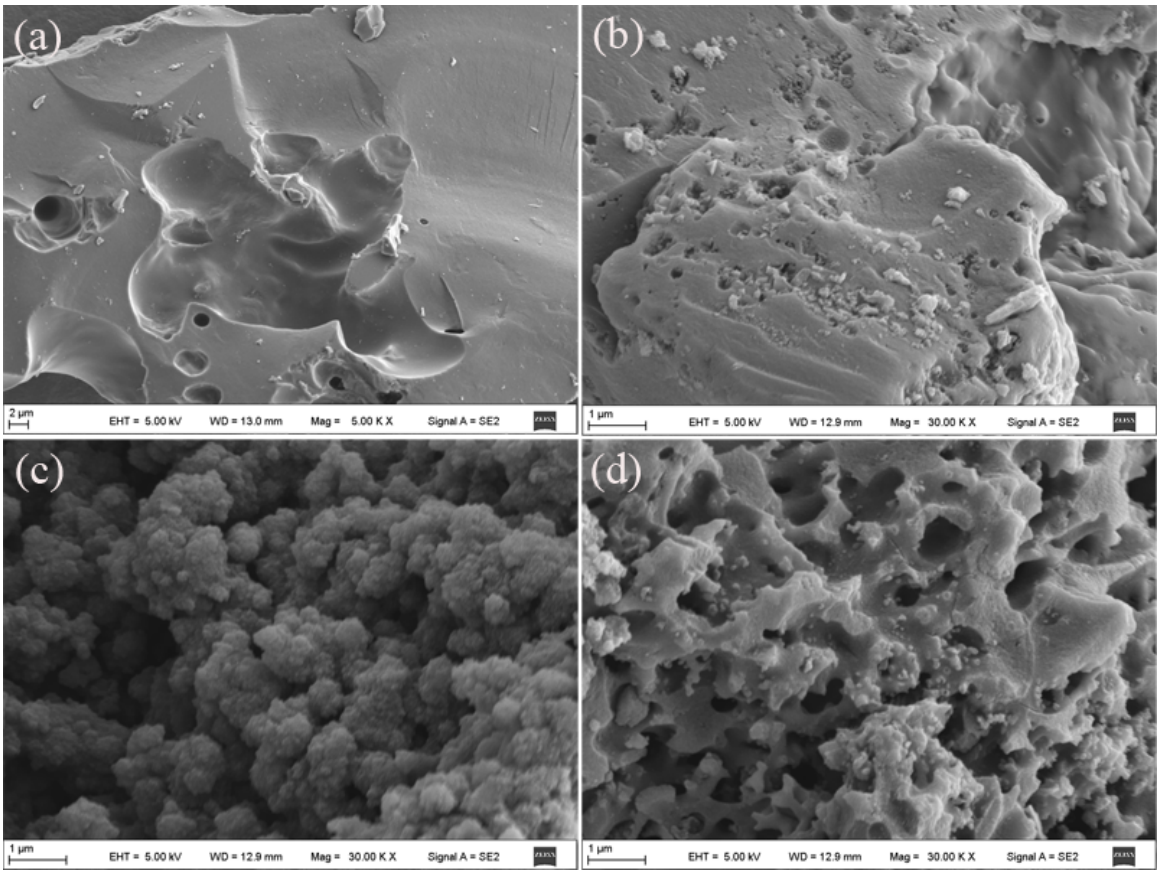

Figure 1. SEM images of N-RCs samples treated with $ZnCl_2$ activating agent in different proportions: (a) N-RC0, (b) N-RC1, (c) N-RC2 and (d) N-RC3, respectively.

Figure 1 shows the typical SEM images of N-RCs carbon samples. The pristine carbon sample of N-RC0 has a smooth monolith surface without apparent pores (Figure 1a). While, as the addition of $ZnCl_2$, the surface morphology of N-RCs samples are changed. The N-RC1 sample exhibits large lumps with an unconspicuous pore structure and rough surface (Figure 1b) when comparing to the N-RC0. More interestingly, as is shown (Figure 1c), the N-RC2 sample presents granular-like morphology, that is composed of interconnected carbon nanospheres, forming loose porous structure and offering sufficient reservoirs for electrolyte, which was desirable for a supercapacitor electrode. Furthermore, the irregular macroporous and loose structure of N-RC3 sample can be observed (Figure 1d). These differences in morphologies reveal that the structural characters of N-RCs samples are seriously affected by the activation ratio during the carbonization process.

The unique structure of N-RC2 sample was further confirmed by TEM (Figure 2). As seen from low-magnification TEM images (Figure 2a), N-RC2 displays a certain amount of pore structure, which is consistent with the result of SEM image analysis. Figure 2b shows high-magnification TEM images indicating that the N-RC2 may present some structural defects and lattice disorder architectures, which would play a significant role in electrolyte ion and charge accommodation region.

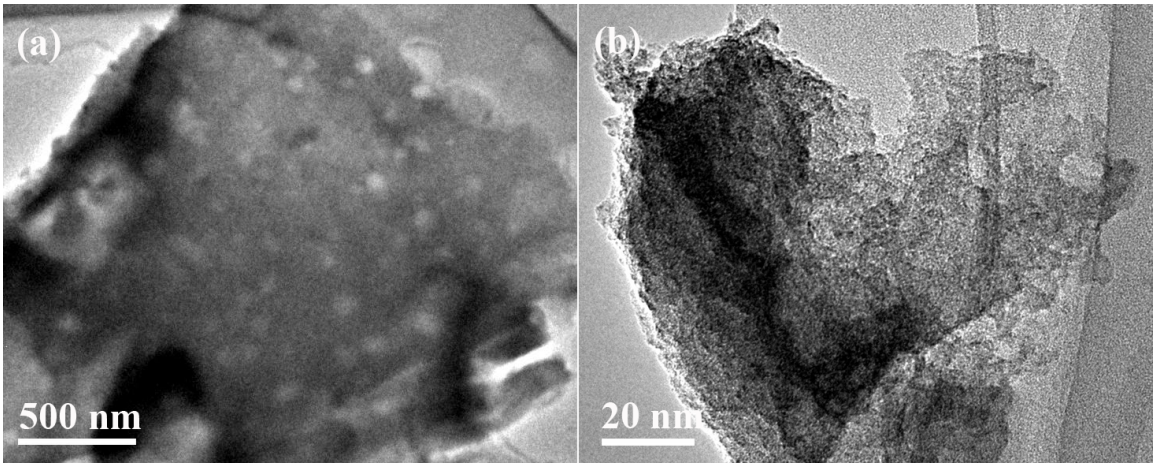

Figure 2. (a), (b) TEM images of N-RC2 sample under different magnifications.

Elemental analysis, BET surface area, and pore structure characterization parameters of N-RCs are summarized in Table 1. Visibly, the $ZnCl_2$-treated samples (N-RC1, N-RC2 and N-RC3) have a higher increase nitrogen content compared to the N-RC0. Specially, a maximum nitrogen content 6.55% is obtained for N-RC2, which can cause an increase in electric conductivity, and concurrently ameliorate surface wettability as well as adsorption properties that facilitate an electrochemical reaction on the carbon surface, thus improving the electrochemical performance. The nitrogen adsorption/desorption isotherms and pore size distribution curves of the carbon samples are shown in Figure 3. It is found that the structural character of samples are significantly affected by the amount of $ZnCl_2$. As shown in Figure 3a, The N-RC0 sample exhibits very low surface area, while, after treated with $ZnCl_2$, the nitrogen adsorption-desorption isotherms of N-RCs (N-RC1, N-RC2, and N-RC3) are presented type IV with a H3 hysteresis loop in the range of ca. 0.45-1.0 P/P_0, which suggests the N-

RCs have mesoporous structures. Meanwhile, at low relative pressure ($P/P_0 < 0.45$), the adsorption isotherms of N-RCs are saturated, indicating the adsorption of micropores. Moreover, pore size distribution and pore volume were evaluated by the Barrett-Joyner-Halenda (BJH) method, and the pore size distributions of N-RCs are shown in Figure 3b. The N-RC0 sample displays a low porosity with a very low N_2 sorption pore volume, while samples treated with $ZnCl_2$ (N-RC1, N-RC2, and N-RC3) show higher pore volumes and a broad pore size distribution in the range of 1 to 100 nm. As is seen in Table 1, the N-RCs show a specific surface area (S_{BET}) increasing from 7.44 to 711.20 $m^2\ g^{-1}$ and a total pore volume in the range of 0.02 to 0.64 $cm^3\ g^{-1}$ during the activation ratios increase from 1:0 to 1:1.5. Particularly, the specific surface area and total pore volume of N-RC2 are 681.6 $m^2\ g^{-1}$ and 0.49 $cm^3\ g^{-1}$, respectively. However, on the contrary, the micropore surface area (S_{mic}) of N-RCs obviously reduced, which may be caused by the collapse and aggregation of some carbon network skeletons in high activation ratio. The large specific surface area and appropriately porous structure are favorable to speed up mass charge transfer and ion diffusion, consequently leading to higher capacitance storage and rate capability [31].

Table 1. The BET measurement and elemental analysis summary of N-RCs samples.

Sample	Element content analysis			S_{BET} [a]	S_{mic} [b]	V_{total} [c]	D [d]
	C%	N%	H%	($m^2\ g^{-1}$)	($m^2\ g^{-1}$)	($cm^3\ g^{-1}$)	(nm)
N-RC0	56.20	4.39	0.81	7.44	-	0.02	11.67
N-RC1	82.06	6.04	1.45	641.00	256.35	0.40	2.46
N-RC2	74.46	6.55	1.54	681.60	136.18	0.49	2.90
N-RC3	74.57	5.53	1.55	711.20	110.17	0.64	3.62

[a]Specific surface area determined according to the BET (Brunauer-Emmett-Teller) method.

[b] Micropore surface area from the t-plot method.

[c] Total pore volume.

[d] Adsorption average pore diameter.

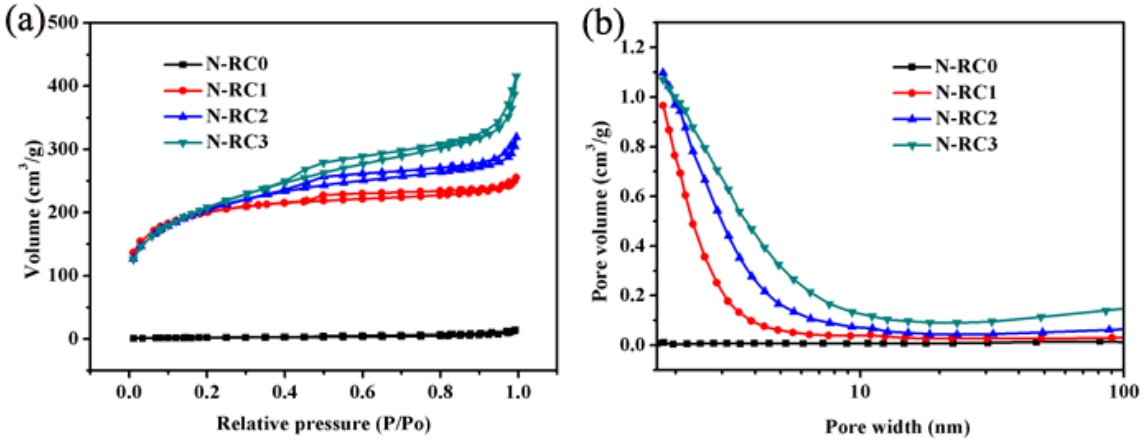

Figure 3. (a) Nitrogen adsorption-desorption isotherms, (b) Pore size distribution curves of the N-RC2 sample, respectively.

Figure 4a shows the XRD patterns of N-RC2 sample. Clearly, two typical broad diffraction peaks at around 22.7° and 42.4° are appeared, ascribing to the (002) and (100) crystal planes of graphitic carbon, respectively, suggesting that the N-RC2 made of graphitic and amorphous carbon [32]. The Raman spectra of the N-RC2 sample is presented in Figure 4b. As can be seen in the spectrum, the sample shows two distinct peaks at around 1347 (D-band) and 1612 cm^{-1} (G-band), respectively. The D-band is a common feature of the disordered carbon/structural defects of the carbon material, while the G-band is closely related to a graphitic carbon phase with an sp^2 electronic conguration, such as graphene layers [33]. In addition, N-RC2 exhibits a strong G-band signal and a slightly lower intensity D-band (I_D/I_G = 0.98), implying that the sample is constituted of turbostratic carbon with a weakly ordered graphitic microstructure, which could pay an important role in charge accommodation, and thus improve the electrical conductivity of materials.

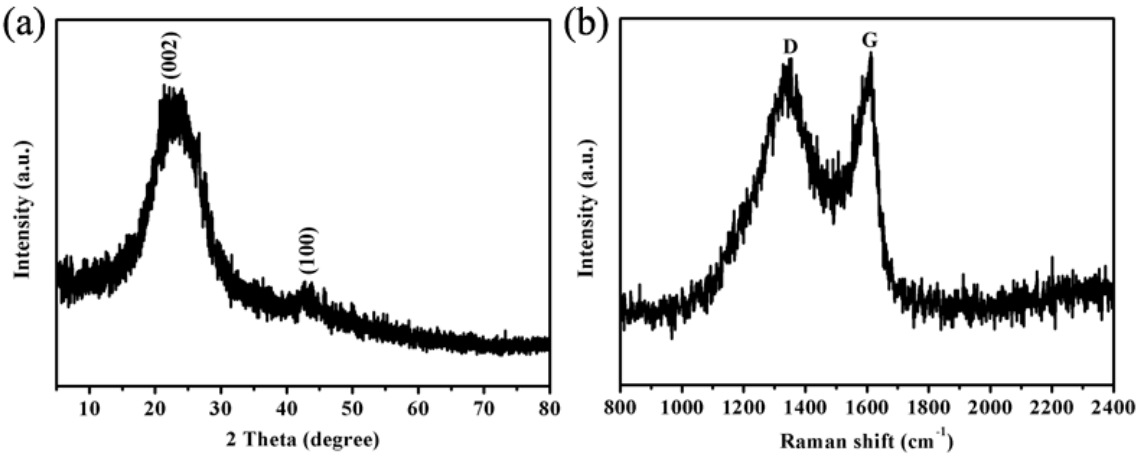

Figure 4. (a) X-ray diffraction pattern and (b) Raman spectrum of N-RC2 sample, respectively.

3.2. Electrochemical characteristics of N-RCs electrodes

The cyclic voltammograms (CVs) of different electrodes were measured at a scan rate of 50 mV s^{-1} in 6 mol L^{-1} KOH electrolyte. Rectangle-like shapes of CV curves are observed that the N-RCs electrodes with different $ZnCl_2$ activating agent at 700 °C (Figure 5a). Clearly, the N-RC2 electrode has a higher specific capacitance than other electrodes, according to the linear relationship between CV curve area and specific capacitance. In addition, the CV curve of N-RC2 electrode retains quasi-rectangular shape even at a scan rate of up to 100 mV s^{-1} (Figure 5b), suggesting the electrode material exhibits a remarkable high rate capability.

The galvanostatic charge/discharge measurement was carried out at various current densities ranging from 0.5 to 8 A g^{-1} within the potential window from -1.0 to 0 V of the N-RC2 electrode, and the results are shown in Figure 5c. The N-RC2 electrode had highly symmetrical GCD curves, indicating that such electrode possesses excellent EDLC characteristic and electrochemical reversibility. The specific capacitance of the electrodes can be calculated using the following formula:

$$C_m = C / m = (I\,t) / (\Delta V\,m) \qquad (1)$$

where C_m is specific capacitance (F g^{-1}), I is charge/discharge current (A), t is the time of discharge (s), ΔV is the voltage difference between the upper and lower potential limits, and m is the mass of the active electrode material. The correlation between the specific capacitance and the different current densities for N-RC2 electrode is calculated accord to the above equation and shown in Figure 5d. The N-RC2 electrode exhibits the highest specific capacitance of 250 F g^{-1} at 0.5 A g^{-1} and 200 F g^{-1} at 8 A g^{-1}, remaining about 80% capacitance retention, suggesting an excellent excellent rate capability.

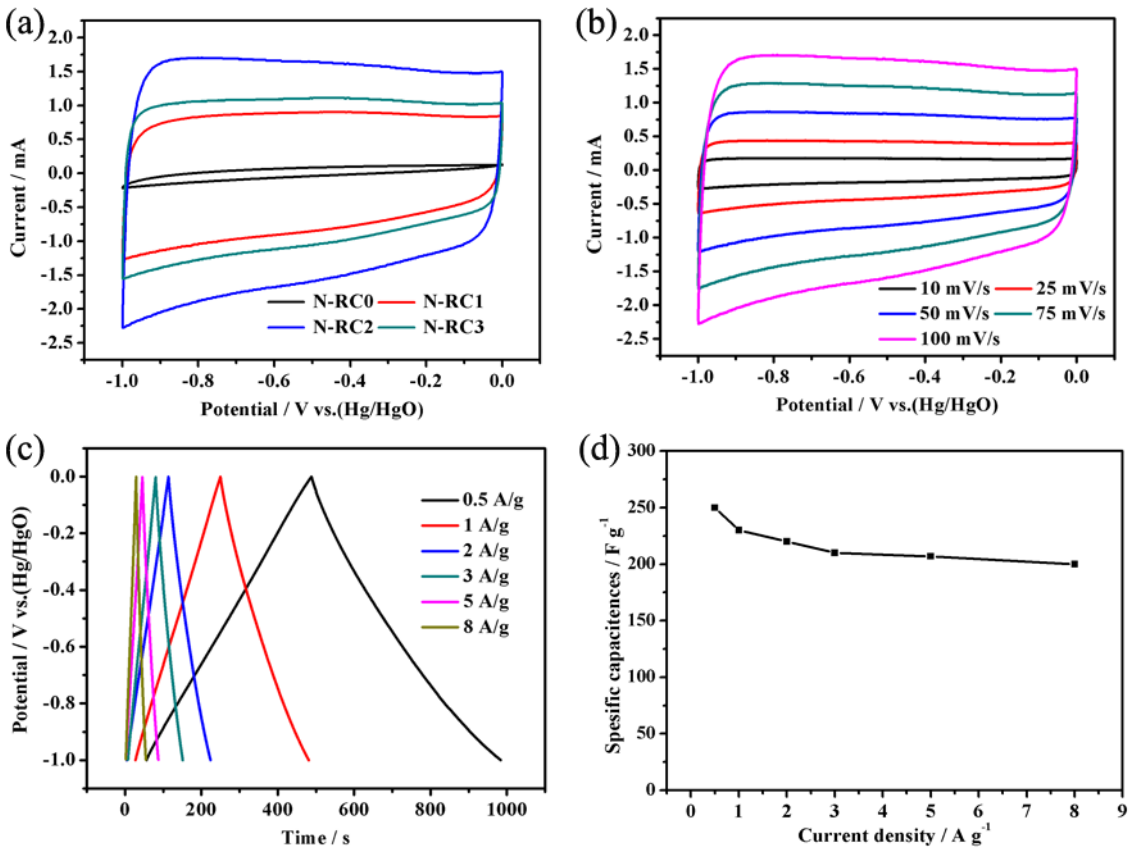

Figure 5. (a) CV curves of N-RCs electrodes synthesized at 700 °C at a scan rate of 50 mV s^{-1}, (b) CV curves of N-RC2 electrode at various scan rates, (c) Galvanostatic charge/discharge curves of N-RC2 electrode at various current densities, (d) Specific capacitance as a function of the current densities of N-RC2 electrode.

Further, we also fabricated two-electrode symmetric supercapacitor to assess the electrochemical performance of N-RC2 electrode. It is reported that the neutral Na_2SO_4 aqueous electrolyte has a higher operation voltage compared to the acid and alkali solutions [34]. Therefore, we assembled the N-RC2//N-RC2 symmetric supercapacitor and characterized its electrochemical performance in 0.5 mol L^{-1} Na_2SO_4 aqueous electrolyte. The as-assembled symmetric cell was first measured at different potential windows from 1.0 to 2.0 V at 50 mV s^{-1}, and the resulting CV curves are exhibited in Figure 6a. when the high voltage extends to 1.8 V, the CV curves of the supercapacitor

still remain rectangular-like shape that indicates ideal capacitive behavior and good reversibility. However, the current is dramatically increased when the voltage reaches to 2.0 V, leading to serious distortion of the CV curve, which because of the electrolyte is being decomposed with hydrogen and/or oxygen evolution [35]. Therefore, we chose the potential window of 1.8 V to measure the electrochemical performance of the symmetric cell. Figure 6b shows the CV curves of the symmetric cell obtained at different scan rates from 10 to 100 mV s^{-1} at the voltage range of 0 to 1.8 V, we can see that the CV curve area increases with increasing scan rate, there is no obvious change and still keep a quasi-rectangular shape even at a scan rate of 100 mV s^{-1}. Galvanostatic charge/discharge curves of the electrode at different current densities from 0.25 to 8 A g^{-1} are displayed in Figure 6c, demonstrating a good capacitive performance of the symmetric cell. The specific energy density (*E*, Wh kg^{-1}) and power density (*P*, W kg^{-1}) for a supercapacitor cell were counted using the following formulas.

$$E = {}^{1}/_{2}CV^{2} \quad (2)$$

$$P = E/t \quad (3)$$

where *C* is the specific capacitance of the cell (F g^{-1}), *V* is the voltage change during the discharge process after the IR drop in galvanostatic discharge curve, *t* is the time of discharge (s).

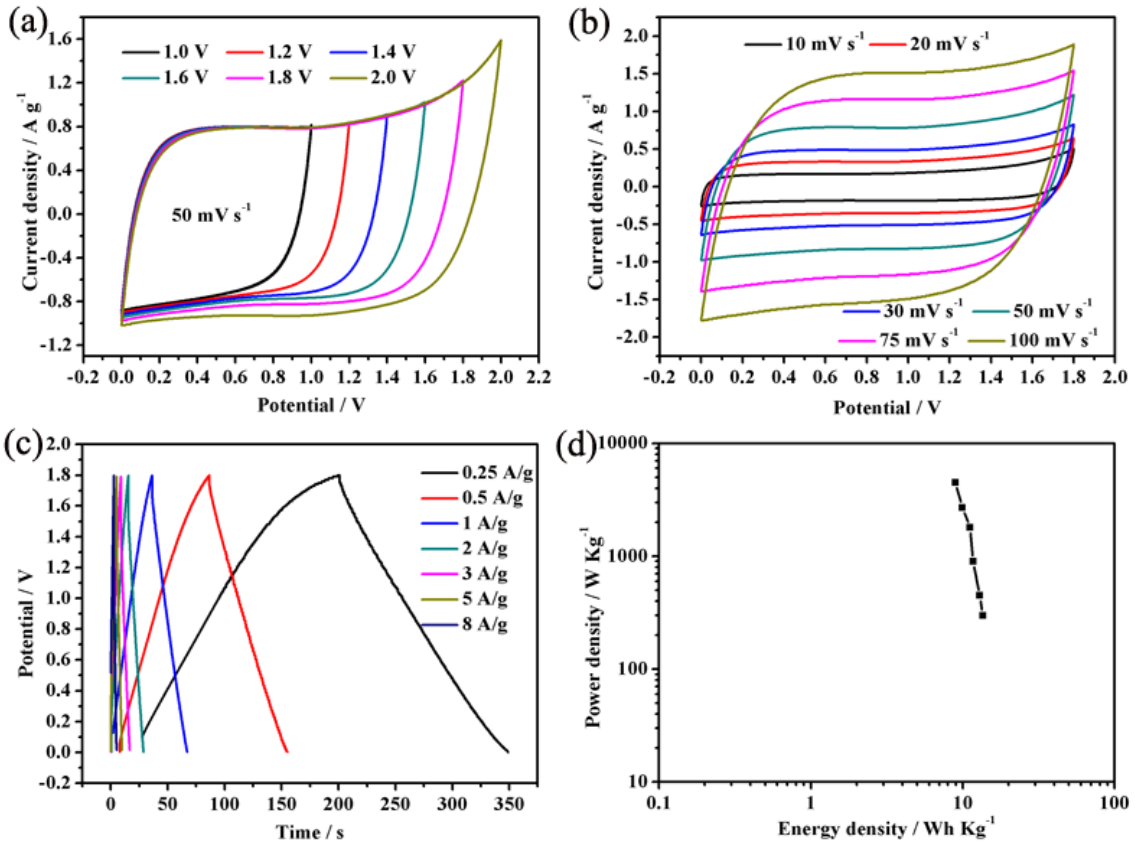

Figure 6. (a) CV curves of N-RC2 symmetric cell at different voltage windows at a scan rate of 50 mV s^{-1}, (b) CV curves of N-RC2 symmetric cell at voltage window of 0 to 1.8 V at various scan rates, (c) Galvanostatic charge/discharge curves of N-RC2 symmetric cell at various current densities, (d) Ragone plot related to energy and power densities of N-RC2 symmetric cell.

Through calculation, the N-RC2//N-RC2 symmetric cell shows the highest energy density is 13.55 Wh kg^{-1} at a power density of 399.80 W kg^{-1} and remained at 5.69 Wh kg^{-1} at a power density of 6401 W kg^{-1}, meaning that the specific energy of electrode material decreases with increasing specific power. Moreover, compared with those previously reported carbon-based aqueous symmetric cells [36-38], the obtained maximum energy density is considerably higher. The Ragone plot of the device describing the relationship between energy density and power density is shown in Figure 6d.

Electrochemical impedance spectroscopy (EIS) measurement was used to gain a deep insight into the resistive and capacitive behavior of the N-RC2//N-RC2 symmetric cell and exhibited in Figure 7a. Analysising the Nyquist plots, the symmetric cell possesses a small ESR of 2.65 Ω, as well as shows obvious semicircle at the high frequency region and a sharp line at the low frequency region, indicating a low charge-transfer resistance in the electrochemical system and a pronounced capacitive behavior with small diffusion resistance. Thus, the symmetric cell has a high electrical conductivity. The cycling stability of N-RC2//N-RC2 symmetric cell was measured by charge/discharge cycling at a constant current density of 5 A g^{-1} for 5000 cycles. As shown in Figure 7b, about 92.8% of the initial capacitance is retained for the symmetric cell, which displays satisfactory cycling stability.

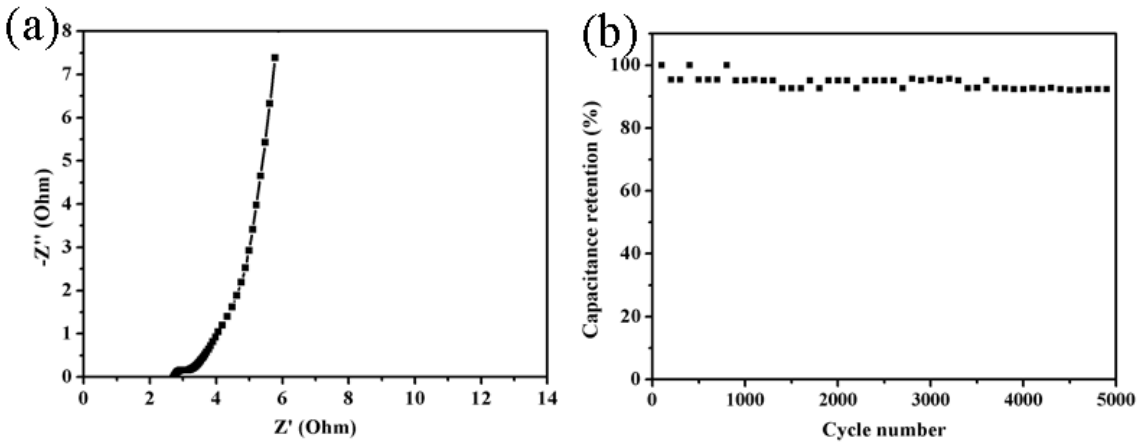

Figure 7. (a) Nyquist plot of N-RC2 symmetric cell, (b) Cycling stability of N-RC2 symmetric cell at 5 A g^{-1}.

4. CONCLUSIONS

In summary, by optimizing the carbonization temperatures and the amount of $ZnCl_2$ activating agent, the resulting porous carbon N-RC2 exhibits a loose, porous morphology, which produce high specific surface area and large pore volume. As an electrode material for supercapacitors, the N-RC2 electrode possess a maximum capacitance of 250 F g^{-1} in three-electrode systems. Furthermore, the as-assembled N-RC2//N-RC2 symmetric supercapacitor device with an wide operation voltage of 0 to 1.8 V in 0.5 mol L^{-1} Na_2SO_4 aqueous electrolyte delivers a high energy density of 13.55 Wh kg^{-1}, and has an excellent cycleability. The outstanding capacitive properties demonstrate that the nitrogen-doped

Rapeseed residues activated carbons (N-RCs) might be a promising candidate for the electrode material of high-performance supercapacitor applications.

ACKNOWLEDGEMENTS
The research was financially supported by the Science and Technology program of Gansu Province (NO.1308RJZA295, 1308RJZA265), the Colleges and Universities Scientific Research Program of Gansu Province (2013B-069), the National Science Foundation of China (NO.21164009, 21174114), the program for Changjiang Scholars and Innovative Research Team in University (IRT1177).

References

1. L. L. Zhang and X. S. Zhao, *Chem. Soc. Rev.*, 38 (2009) 2520-2531.
2. B. You, J. H. Jiang and S. J. Fan, *ACS Appl. Mater. Inter.*, 6 (2014) 15302-15308.
3. L. Hao, X. L. Li and L. J. Zhi, *Adv. Mater.*, 25 (2013) 3899-3904.
4. C. L. Long, T. Wei, J. Yan, L. L. Jiang and Z. J. Fan, *ACS Nano*, 7 (2013) 11325-11332.
5. S. M. Chen, R. Ramachandran, V. Mani and R. Saraswathi, *Int. J. Electrochem. Sci.*, 9 (2014) 4072-4085.
6. Y. W. Zhu, S. Murali, M. D. Stoller, K. J. Ganesh, W. Cai, P. J. Ferreira and R. S. Ruoff, *Science*, 332 (2011) 1537-1541.
7. W. H. Lee and J. H. Moon, *ACS Appl. Mater. Inter.*, 6 (2014) 13968-13976.
8. H. Peng, G. F. Ma, K. J. Sun, J. J. Mu, Z. Zhang and Z. Q. Lei, *ACS Appl. Mater. Inter.*, 6 (2014) 20795-20803.
9. B. Xu, H. Duan, M. Chu, G. P. Cao and Y. S. Yang, *J. Mater. Chem. A.*, 1 (2013) 4565-4570.
10. Y. S. Yun, S. Y. Cho, J. Shim, B. H. Kim, S. J. Chang, S. J. Baek and H. J. Jin, *Adv. Mater.*, 25 (2013) 1993-1998.
11. J. H. Lee, N. Park, B. G. Kim, D. S. Jung, K. Im, J. Hur and J. W. Choi, *ACS Nano*, 7 (2013) 9366-9374.
12. J. Jiang, Y. Y. Li, J. P. Liu, X. T. Huang, C. Z. Yuan and X. W. D. Lou, *Adv. Mater.*, 24 (2012) 5166-5180.
13. K. J. Sun, H. P. Wang, H. Peng, Y. J. Wu, G. F. Ma and Z. Q. Lei, *Int. J. Electrochem. Sci.*, 10 (2015) 2000-2013.
14. H. C. Chen, F. G. Sun, J. T. Wang, W. C. Li, W. M. Qiao, L. C. Ling and D. H. Long, *J. Phys. Chem. C.*, 117 (2013) 8318-8328.
15. W. H. Lee and J. H. Moon, *ACS Appl. Mater. Inter.*, 6 (2014) 13968-13976.
16. M. Zhou, F. Pu, Z. Wang and S. Y. Guan, *Carbon*, 68 (2014) 185-194.
17. J. Zhou, Z. S. Zhang, W. Xing, J. Yu, G. X. Han, W. J. Si and S. P. Zhuo, *Electrochim. Acta.*, 153 (2015) 68-75.
18. Z. H. Guo, Q. W. Zhou, Z. J. Wu, Z. G. Zhang, W. Zhang, Y. Zhang, L. J. Li, Y. Gao, Z. Z. Cao, H. Wang and Y. F. Gao, *Electrochim. Acta.*, 113 (2013) 620-627.
19. Z. J. Zhang, C. Chen, P. Cui and X. Y. Chen, *J. Power Sources*, 242 (2013) 41-49.
20. T. T. Zhu, J. Zhou, Z. H. Li, S. J. Li, W. J. Si and S. P. Zhuo, *J. Mater. Chem. A.*, 2 (2014) 12545-12551.
21. B. Xu, S. S. Hou, F. L. Zhang, G. P. Cao, M. Chu and Y. S. Yang, *J. Electroanal. Chem.*, 712 (2014) 146-150.
22. D. H. Jurcakova, M. Seredych, G. Q. Lu and T. J. Bandosz, *Adv. Funct. Mater.*, 19 (2009) 438-447.
23. Q. Xu, X. L. Yu, Q. H. Liang, Y. Bai, Z. H. Huang and F. Y. Kang, *J. Electroanal. Chem.*, 739 (2015) 84-88.

24. T. E. Rufford, D. Hulicova-Jurcakova, E. Fiset, Z. H. Zhu and G. Q. Lu, *Electrochem. Commun.*, 11 (2009) 974-977.
25. L. Wei and G. Yushin, *Nano Energy*, 1 (2012) 552-565.
26. P. P. M. Fung, W. H. Cheung and G. McKay, *Chinese J. Chem. Eng.*, 20 (2012) 497-504.
27. H. L. Wang, Z. W. Xu, A. Kohandehghan, Z. Li, K. Cui, X. H. Tan and D. Mitlin, *ACS Nano*, 7 (2013) 5131-5141.
28. M. J. Zhi, F. Yang, F. K. Meng, M. Q. Li, A. Manivannan and N. Q. Wu, *ACS Sustain. Chem. Eng.*, 2 (2014) 1592-1598.
29. H. Peng, G. F. Ma, K. J. Sun, J. J. Mu, Z. Zhang and Z. Q. Lei, *J. Phys. Chem. C.*, 118 (2014) 29507-29516.
30. H. Peng, G. F. Ma, K. J. Sun, J. J. Mu, Z. Zhang and Z. Q. Lei, *ACS Appl. Mater. Inter.*, 6 (2014) 20795-20803.
31. K. Fic, G. Lota, M. Meller and E. Frackowiak, *Energy Environ. Sci.*, 5 (2012) 5842-5850.
32. P. P. Su, L. Jiang, J. Zhao, J. W. Yan, C. Li and Q. H. Yang, *Chem. Commun.*, 48 (2012) 8769-8771.
33. M. S. Dresselhaus, A. Jorio, M. Hofmann, G. Dresselhaus and R. Saito, *Nano Lett.*, 10 (2013) 751-758.
34. Q. Wang, J. Yan, Y. B. Wang, T. Wei, M. L. Zhang, X. Y. Jing and Z. J. Fan, *Carbon*, 67 (2014) 119-127.
35. Y. P. Zhai, Y. Q. Dou, D. Y. Zhao, P. F. Fulvio, R. T. Mayes and S. Dai, *Adv. Mater.*, 23 (2011) 4828-4850.
36. L. Demarconnay, E. Raymundo-Pinero and F. Béguin, *Electrochem. Commun.*, 12 (2010) 1275-1278.
37. X. J. He, R. C. Li, J. S. Qiu, K. Xie, P. H. Ling, M. X. Yu, X. Y. Zhang and M. D. Zheng, *Carbon*, 50 (2012) 4911-4921.
38. Q. Wang, J. Yan, T. Wei, J. Feng, Y. M. Ren, Z. J. Fan, M. L. Zhang and X. Y. Jing, *Carbon*, 60 (2013) 481-487.